In situ polymerization of bisphenol-A-carbonate cyclic oligomers in miscible blends with a styrene–acrylonitrile copolymer: phase separation dynamics and the influence of phase dispersion on ductility

Warren L. Nachlis*†, Roger P. Kambour*‡ and William J. MacKnight†
* *General Electric Corporate Research and Development, Schenectady, NY 12301, USA*
† *Polymer Science and Engineering Department, University of Massachusetts, Amherst, MA 01003, USA*
(Received 1 December 1993)

The *in situ* polymerization of bisphenol-A-carbonate cyclic oligomers (BPACY)/styrene–acrylonitrile copolymer (SAN) blends has been demonstrated to yield PC/SAN blends with morphologies unattainable via conventional melt blending. Extremely fine phase dispersion can be obtained by this method of blend preparation. Domain-coarsening kinetics have been shown to be quite sensitive to the volume fraction of the dispersed phase. The 'pinning' of domain coarsening, unique to polymer systems, can be attributed to the extreme barriers to diffusive coarsening mechanisms in these systems. Thus, phase coarsening is arrested when percolation ceases or domains no longer form local clusters. The dispersed phase size has been shown to have a dramatic effect on high-stress deformation in systems where a brittle phase is dispersed in a more compliant ductile matrix. The increased ductility of blends with finer phase dispersions has been rationalized based on a lower tendency for smaller brittle phases to craze and crack in addition to the influence of complex local stress fields in heterogeneous materials.

(Keywords: blend; morphology; *in situ* polymerization)

INTRODUCTION

Although most polymer blend research has focused on materials prepared by conventional mixing of constituent high-molecular-weight polymers[1–6], the *in situ* formation of blends via the polymerization of a monomer within a polymeric matrix has occasionally been explored[7–31]. The most commercially significant example of *in situ* blend formation is found in the toughening of polymers by rubber modification[7].

The process of *in situ* blend formation is most easily understood by considering the schematic three-component phase diagram in *Figure 1*. The shaded region represents the single-phase region, while the area below the curve denotes compositions at which two phases exist at equilibrium. The compositions of these phases are given by the intersection of the corresponding tie line with the phase boundary. Relative phase volumes can be determined by the 'lever rule'[14–16]. *In situ* blend formation begins with a homogeneous mixture of a monomer and polymer, point C in *Figure 1*. When polymerization begins, the system progresses down the reaction coordinate CD. Phase separation begins when the reaction coordinate intersects the phase boundary. A series of tie lines could, in theory, be constructed to give phase compositions as the polymerization progresses. However, the kinetics of the processes involved usually preclude the attainment of equilibrium until polymerization is completed. This is represented by

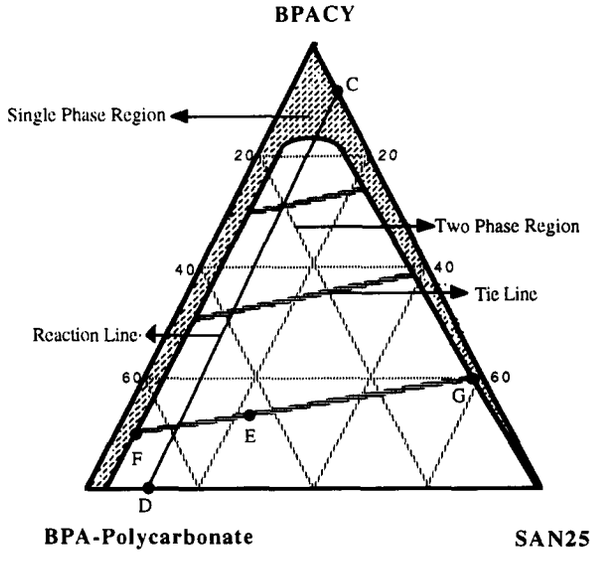

Figure 1 Schematic phase diagram for *in situ* blend formation

‡ To whom correspondence should be addressed

0032-3861/94/17/3643–15

point D, where a heterogeneous blend is obtained. The morphology of the final product is determined by the complex interplay of polymerization kinetics, phase equilibria and phase separation kinetics.

In addition to the *in situ* formation of thermoplastic blends, interpenetrating polymer networks (IPNs) are another example of a multicomponent polymer system prepared *in situ*. Most IPNs are formed by synthesizing and/or crosslinking one network in the immediate presence of another. The existence of crosslinks (chemical and/or physical) in these systems defines them as a particular class of blends prepared *in situ*. Sperling has reviewed this active research area[32,33]. Although neither grafting nor crosslinking occurs in the systems described in this work, their relationship to other similar systems is noted.

The work described here explores the use of bisphenol-A-carbonate cyclic oligomers (BPACY) as novel building blocks for polymer blends. The *in situ* polymerization of these reactive oligomers from an initially homogeneous mixture with a styrene–acrylonitrile copolymer and control of incipient liquid–liquid phase separation enabled the preparation of materials with variable but controlled morphologies. The morphology-coarsening kinetics were investigated in a system where isothermal phase separation occurs due to polymerization of one component of an initially homogeneous mixture. Finally, these materials were used to investigate the relationship between morphology and high-stress deformation behaviour of materials in which a stiff brittle phase is dispersed in a more compliant ductile matrix.

It has been proposed that the failure energy of a ductile polymer can be increased by dispersing in it a higher modulus brittle polymer[34,35]. The concept is based on the fact that the otherwise brittle dispersed particle will absorb a significant amount of energy if it can be induced to undergo shear flow along with the matrix instead of brittle failure. This mechanism rests on the assumption that the stress field around the otherwise brittle dispersed particle in a more compliant matrix is substantially different from that which is encountered when a monolithic specimen of the material is under stress.

When a stress is applied to a heterogeneous material, the microscopic stress fields may be very different from the global stresses[6]. An early approach to this problem considered the case of an isolated spherical particle embedded in an isotropic solid body[36]. The model developed by Goodier assumes perfect adhesion at the interface between phases and treats only the linear elastic behaviour, to yield the classical closed form solution. A global uniaxial tensile stress results in a local triaxial stress state around the inclusion due to differences in the elastic constants between the two phases. The magnitude of the stress concentration factor (SCF), expressed as the ratio of major local principal stress to applied stress, as well as the location of its maximum are determined by the disparities in elastic constants (modulus and Poisson's ratio) between the two phases; the larger the differences, the higher is the SCF. When the inclusion is significantly more compliant than the matrix, the maximum principal stress, major principal strain, maximum dilation, maximum distortion strain energy density and major principal shear stress are all located at 90° to the applied stress at the interface between the matrix and inclusion. These maxima shift, although to varying degrees, toward the polar regions of the inclusion (0° to the applied stress) when the inclusion is less compliant than the matrix[36,37]. When a stiff material is dispersed in a more compliant matrix with a higher Poisson's ratio the tendency for cavitation is reduced in the dispersed phase due to a resolved hydrostatic compression[34,35]. Thus a ductile–brittle transition may be observed due to resolved stress fields as discussed above. The sensitivity of the deformation mechanisms of homogeneous materials to the details of the stress field has been discussed by Sternstein[38] while others have demonstrated that polymers that are characterized by brittle behaviour under uniaxial tension deform via ductile yielding when the hydrostatic component of the stress tensor is compressive[39–43].

This concept has been demonstrated by others for dispersions of brittle styrene–acrylonitrile copolymers (SAN) in ductile PC matrices[34,35]. Koo *et al.*[44] extended this concept to other combinations. The importance of the size of the dispersed phase as well as the strength of the interface was demonstrated by Angola *et al.*[45]. The addition of a compatibilizer, poly(styrene-*co*-maleic anhydride), to a nylon-6/SAN system reduced the size of the dispersed SAN phase and improved the interfacial strength yielding a material with superior tensile and impact strengths. Although detailed analysis of the deformation mechanisms was not performed, the size of the dispersed phase, interfacial strength as well as the details of the components' crazing and shear yielding envelopes under triaxial stress fields are clearly determining factors of a blend's mechanical performance.

The effect of dispersed phase size has also been demonstrated by several other investigations. Quintens *et al.*[46–48] demonstrated that annealing injection-moulded PC/SAN blends above the glass transition temperature (T_g) of both components results in a dramatic coarsening of the phase dispersion[45–47]. The coarsening of the morphology was accompanied by a loss in ductility. Kim and Lee[49] have shown that the addition of a compatibilizer, poly(ε-caprolactone), to PC/SAN blends reduces the size of the dispersed SAN phase yielding improved tensile and notched Izod impact strengths[49]. Finally, co-extruded microlayer sheet consisting of alternating layers of PC and SAN has been studied[49–52]. Most relevant is the effect of layer thickness on the deformation behaviour of these sheets. At constant composition and an overall sheet thickness of 1.2 mm, the number of layers was varied from 49 to 776. Thus layer thicknesses varied from 24 μm to 1.6 μm. When the layers were thick, the components displayed behaviour characteristic of the homogeneous bulk polymers (i.e. the SAN crazed or cracked while the PC deformed primarily via shear yielding). However, as the layers became thinner, crazing in the SAN was suppressed and the SAN also deformed via shear yielding. The change in deformation behaviour of the SAN was attributed to changes in stress state due to the impingement of PC shear bands[51].

EXPERIMENTAL

The synthesis and polymerization of BPACY have recently been reported[53–57]. BPACYs are synthesized via an interfacial hydrolysis/condensation of bisphenol-A-bis(chloroformate) (see *Figure 2*). The isolated cyclic oligomers have a $M_w = 1529$ (absolute molecular weight via high-performance liquid chromatography (h.p.l.c.)) and contain less than 0.05% linear contaminants. These

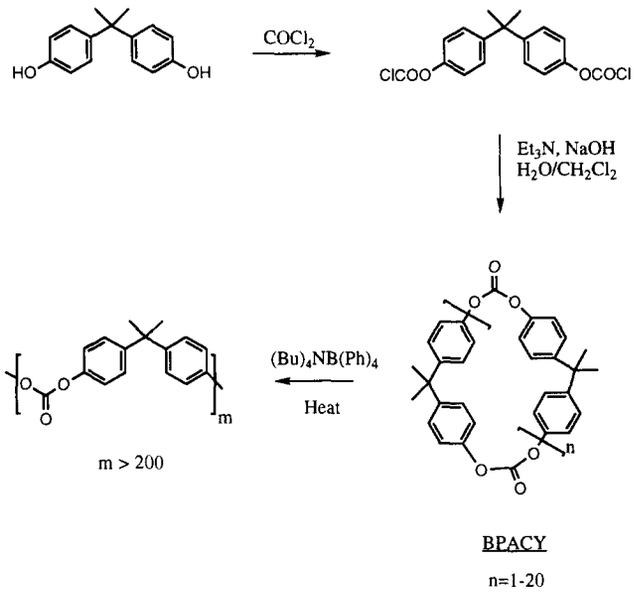

Figure 2 Synthesis and polymerization of bisphenol-A-carbonate cyclic oligomers

oligomers can be isolated as an amorphous material with $T_g = 147°C$ and a density of 1.197 g cm^{-3}. Rapid polymerization of BPACY to form linear high-molecular-weight bisphenol-A-polycarbonate can be achieved by heating the cyclic oligomers to, for example, 260°C, in the presence of a catalyst such as tetrabutylammonium tetraphenylborate ($(Bu)_4NH(Ph)_4$)]. The properties of the linear polycarbonate prepared in this way are indistinguishable from those of conventional polycarbonate.

The BPACY, linear high-molecular-weight polycarbonate (PC), ($(Bu)_4NB(Ph)_4$) as well as the sytrene–acrylonitrile copolymer used in this study were provided by General Electric Corporate Research and Development. The styrene–acrylonitrile copolymer (SAN25) contained 25 wt% acrylonitrile and had $M_w = 118\,000$ with $M_w/M_n = 2.6$. Blends of BPACY/SAN25 containing $(Bu)_4NB(Ph)_4$ were prepared by co-dissolving components (15% solids) in liquid-chromatography-grade methylene chloride, filtering to remove particulate impurities greater than 0.2 μm, and removal of the solvent by rotary evaporation.

Samples for characterizing the kinetics of morphological coarsening upon *in situ* polymerization of the BPACY were prepared by pressing the powder, prepared as described above, between sheets of Teflon-coated aluminium foil in a compression-moulding press at 260°C. Specimens were heat-treated for different times and then quenched in a water-cooled press with 25°C platen temperatures. Final specimen thicknesses were between 0.08 and 0.1 cm. The sheets prepared as above were not suitable for mechanical property measurements due to the presence of voids. Therefore, a different, two-step, process was used to prepare materials for mechanical property investigations. The powder obtained via solution mixing was first compression-moulded into void-free plaques (8.9 cm × 12.7 cm × 0.1 cm) using a closed mould (160°C, 500 pounds per square inch (psi), 120 s). No conversion of the BPACY to polymer occurred during this stage of the heat treatment, as shown by gel-permeation chromatography (g.p.c.). These plaques were then heat-treated for different periods of time in an open frame mould (8.9 cm × 12.7 cm × 0.08 cm) between Ferrotype plates in a compression moulding press (260°C, 500 psi) and then quenched in a water-cooled press (25°C platen temperature). Some 'flashing' and associated flow occurred during this stage; the effect of this flow on the morphology of the surface of these plaques will be discussed later.

Polymerization kinetics were followed by g.p.c. analysis. A Waters 590 pump, WISP 710b autoinjector, and Styragel columns (10^4, 10^3, 500, 100 Å pore sizes) using chloroform as the mobile phase were used for g.p.c. analyses. A dual detector system was used: Waters 410 differential refractometer in series with a Miran 1A CVF (Foxboro Instruments) infra-red detector (Spectra-Tech 1 mm path length flow cell). The infra-red detector was operated at a wavelength of 5.65 μm (carbonate C=O stretch) where there is no interference from SAN25 absorptions. This enabled the carbonate (cyclic oligomer or polymer) molecular weight distribution to be calculated without interference from the SAN. These components were interfaced with a Nelson Analytical Model 2600 chromatography data station used for data reduction. Unless otherwise noted, molecular weights are relative to polystyrene standards. Glass transition temperatures were determined using a Perkin–Elmer DSC-7 at a heating rate of 20°C min^{-1}.

Tensile specimens were prepared by cutting the 8.9 cm × 12.7 cm × 0.08 cm plaques into dogbone test specimens with 1 cm gauge lengths and 1.3 cm tabs. Specimen edges were carefully polished using a 240 grit rubberized silicon carbide abrasive before testing. Tensile tests were performed on a screw-driven Instron 4500 materials testing frame in conjunction with Instron Series IX computer data acquisition. Arrested cleavage crack tips were prepared by mounting specimens that had been notched with a razor blade in a vice and slowly forcing open the notch using a wedge.

In order to compare the morphologies obtained via *in situ* polymerization to those obtained via conventional melt blending of high-molecular-weight polymers, a 50/50 blend of SAN25 with PC ($M_w = 42\,000$ with $M_w/M_n = 2.4$) was coextruded using a twin-screw extruder at 260°C. This blend was then compression moulded at 260°C for 90 s.

Several microscopic techniques were used to analyse morphologies as well as high-stress deformation mechanisms. Samples for transmission electron microscopy (TEM) were sectioned (0.12–0.15 μm) at room temperature using a Reichert Ultracut E ultramicrotome. A Hitachi H-600 TEM was used to image unstained sections, wherein contrast arises from the electron density difference between phases. Samples for reflected light microscopy were prepared by either facing specimens with a ultramicrotome or polishing to a 1 μm diamond finish prior to oxygen plasma etching. The oxygen plasma etching provides excellent surface relief due to the faster etching rate of polycarbonate relative to SAN25. Surfaces were then sputter-coated with a thin layer of Au/Pd and imaged using a Zeiss Axiovert Metallograph using both reflected bright-field and reflected dark-field illumination. Thin sections (35–40 μm thick) for transmitted light microscopy were prepared by standard grinding and polishing techniques[58]. These specimens were imaged using a Zeiss Photomicroscope in bright-field polarized transmission with and without crossed polars.

RESULTS AND DISCUSSION

In situ *polymerization*

Four requirements must be met for the successful control of phase dispersion via *in situ* polymerization of BPACY. First, a miscible BPACY/polymer combination must be used. Second, the polymerization kinetics of the BPACY dispersed in the host polymer must be rapid relative to the dynamics of phase separation. Third, polymer–polymer phase separation must ensue. Finally, morphologies far from equilibrium must be susceptible to kinetic trapping. Blends of BPACY and SAN25 were found to be miscible across the entire composition range as evidenced by a single composition-dependent T_g (see *Figure 3*). This contrasts with the two-phase behaviour of blends of SAN25 with high-molecular-weight PC (e.g. ref. 58).

With the first and third requirements met, the polymerization kinetics of BPACY/SAN25 blends were investigated. In *Figure 4*, the time dependence of the conversion of BPACY to PC in an SAN25 blend is shown. Under these conditions the polymerization of BPACY was complete in just over 60 s. The PC obtained had $M_w = 39000$ and $M_w/M_n = 2.6$ with less than 0.25% BPACY remaining after polymerization. The molecular weight obtained was equal to or greater than those of most commercial PC resins. Polymerization kinetics, as well as final PC molecular weights for other mixtures with BPACY compositions between 10 and 90 wt%, were quite similar with complete conversion achieved in less than 80 s in all cases.

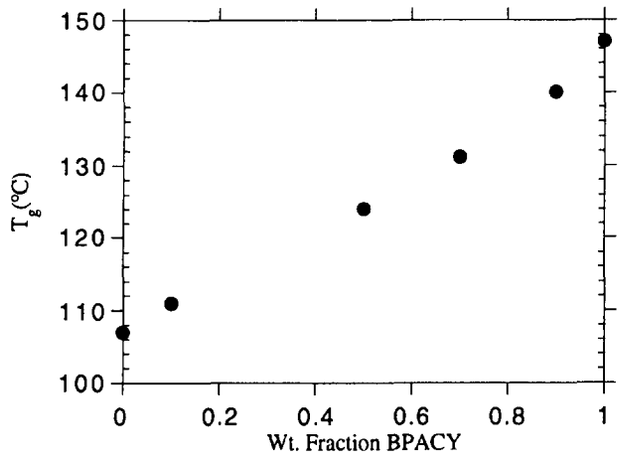

Figure 3 T_g vs. composition of BPACY/SAN25 blends

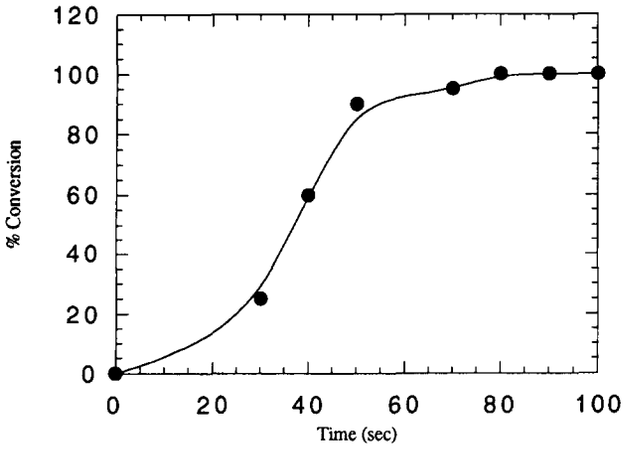

Figure 4 Polymerization kinetics of 50/50 BPACY/SAN25 blends containing 0.07 mol% $(Bu)_4NH(Ph)_4$ (260°C)

Figures 5a to *g* display the morphologies obtained from 50/50 BPACY/SAN25 blends that were heat-treated at 260°C for times between 30 and 600 s before being quenched below T_g. The mixture is still homogeneous after 30 s (*Figure 5a*) when approximately 20% of the cyclics have been converted to polymer. Phase separation is obvious after 60 s (90% BPACY conversion). At this point a SAN25-rich phase is dispersed in a PC matrix (see *Figure 5b*). The PC-rich phase appears dark in TEM micrographs because of its greater electron density relative to SAN25. After 90 s conversion to PC is complete and a phase inversion has occurred resulting in a dispersion of a PC-rich phase in a continuous SAN-rich phase (see *Figure 5c*). At 50 wt% PC, the SAN-rich phase is expected to be continuous because of its greater specific volume. The PC-rich dispersions coarsen over time at 260°C (see *Figures 5d* to *g*).

The morphology of a conventional polymer–polymer melt blend is shown in *Figure 6*. For comparison, the morphology of the blend polymerized *in situ* for 90 s is shown in *Figure 7* at the same magnification. The size of the domains obtained via *in situ* polymerization is ca. 100 times smaller than the size of domains obtained via conventional melt blending.

The glass transitions of the blends described above were characterized by differential scanning calorimetry (d.s.c.) (*Figure 8*). The 30 s sample had a single T_g, which is consistent with the single-phase nature of *Figure 5a*. The d.s.c. results for samples which had been heat-treated for times between 60 and 600 s reveal that equilibrium phase compositions are established rapidly as evidenced by the lack of further change of the T_gs in this time range. That is, the observed phase coarsening occurs at constant phase composition in this time range. Also shown in *Figure 8* are the results for the conventional melt blend, which are identical to those obtained for the *in situ* polymerized blends. Thus *in situ* polymerization does not result in an enhanced miscibility between PC and SAN relative to the conventionally prepared melt-mixed blend. Both methods of blend preparation yield a two-phase system consisting of essentially pure PC and pure SAN domains.

Phase-coarsening kinetics

The phase-coarsening kinetics of blends polymerized *in situ* were investigated over a range of BPACY compositions. Particle size distributions were determined by digital image analysis of TEM micrographs. The number-average radius, R, of dispersed domains is plotted as a function of time in *Figure 9* for blends containing 10, 50, 70 and 90 wt% BPACY. The data have been fit to a scaling relationship of the form

$$R(t) \propto t^{\alpha} \tag{1}$$

where α is varied to provide a best fit. The error bars in *Figure 9* represent the standard deviations of the number-average radii distributions. The rate at which dispersed phases coarsen is seen to be a strong function of the weight (or volume) fraction of the dispersed phase. The scaling exponent, α, is largest when the dispersed phase volume is largest (i.e. 50/50 and 70/30). Domain coarsening was significantly slower at 10/90, $\alpha = 0.33$,

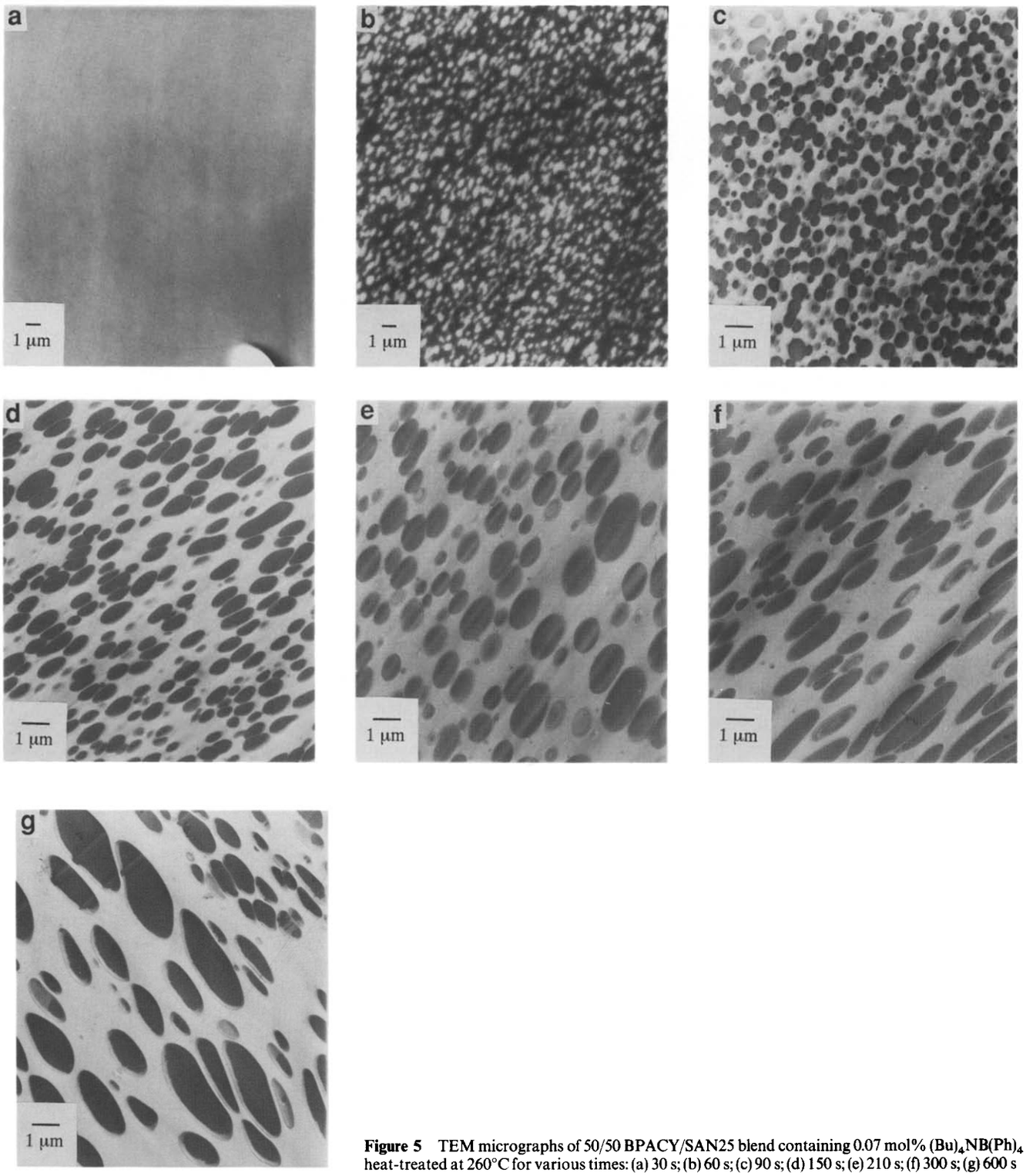

Figure 5 TEM micrographs of 50/50 BPACY/SAN25 blend containing 0.07 mol% $(Bu)_4NB(Ph)_4$ heat-treated at 260°C for various times: (a) 30 s; (b) 60 s; (c) 90 s; (d) 150 s; (e) 210 s; (f) 300 s; (g) 600 s

while at 90/10 the domains do not coarsen at all over time, i.e. $\alpha = 0$.

The demixing of a binary or pseudo-binary mixture due to a rapid change in the thermodynamic stability can occur via one of two mechanisms: (1) nucleation and growth or (2) spinodal decomposition[60–66]. Although the resulting equilibrium structure (two macroscopic liquid phases of $(\phi_1)_{A,eq}$, the equilibrium composition of component 1 in phase A at equilibrium, and $(\phi_1)_{B,eq}$, the equilibrium concentration of component 1 in phase B at equilibrium) is independent of the mechanism of demixing, the intermediate demixed structures may be quite different.

Definitive conclusions regarding the mechanism of demixing under particular experimental conditions can only be drawn from a careful analysis of the early stages of demixing during which equilibrium phase compositions are reached. However, the coarsening processes that occur after equilibrium phase compositions are reached are independent of the mechanism active

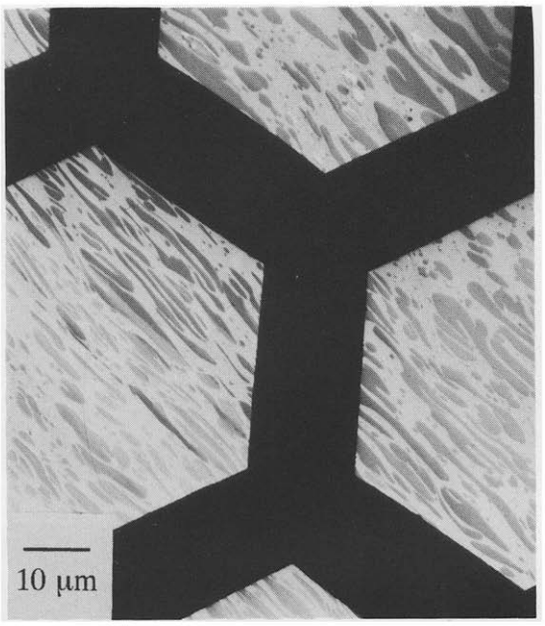

Figure 6 TEM micrograph of 50/50 PC/SAN25 conventional melt blend. (Note that copper grid bars are visible at this magnification)

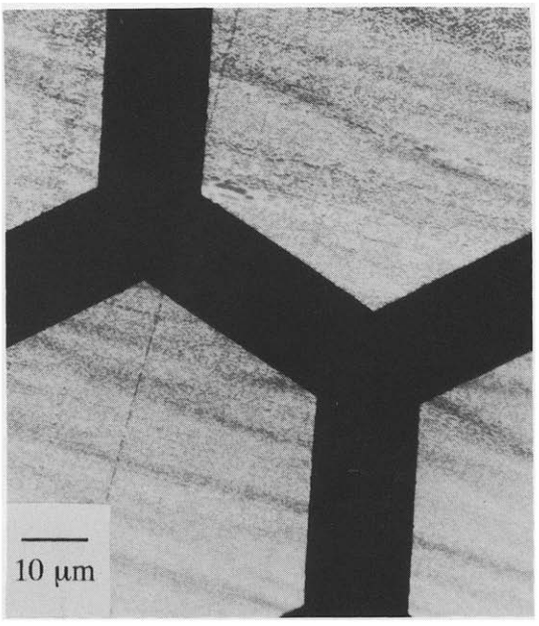

Figure 7 TEM micrograph of 50/50 BPACY/SAN25 blend containing 0.07 mol% $(Bu)_4NB(Ph)_4$ heat-treated at 260°C for 90 s. (Same magnification as *Figure 6*; note that copper grid bars are visible)

during the early stages of demixing[60–66]. The dynamics of these universal coarsening processes are characterized by performing scaling analyses on the average size of dispersed domains by either observing the average radius as a function of time, $R(t)$, when direct real-space images are available or by analysis of the wavenumber of maximum scattered intensity as a function of time, $q_m(t)$, when radiation scattering is used to monitor demixing kinetics. The comparison of the scaling exponents, α, in

$$R(t) \propto t^{\alpha} \tag{2}$$

or

$$q_m(t) \propto t^{-\alpha} \tag{3}$$

with those predicted theoretically provides insights into the physics of the coarsening mechanism.

One of the earliest proposed mechanisms for the coarsening of dispersed domains is referred to as Ostwald ripening[66–68]. The physics of this process is based on an evaporation–condensation mechanism in which larger droplets grow at the expense of smaller ones driven by the lower surface tension of droplets with larger radii. The domains do not, themselves, undergo translation. Instead, diffusion is biased from smaller particles into the matrix as well as diffusion from the matrix into larger particles due to the higher chemical potential of smaller particles (i.e. higher surface tensions) relative to larger particles. Thus, there is a net flux of material from smaller particles through the matrix into larger particles. This theory predicts $\alpha = 1/3$. Scaling exponents of 1/3 have been observed in the late stage of phase coarsening of binary metal alloys and small molecule fluid mixtures[62]. The relevance of this mechanism to the

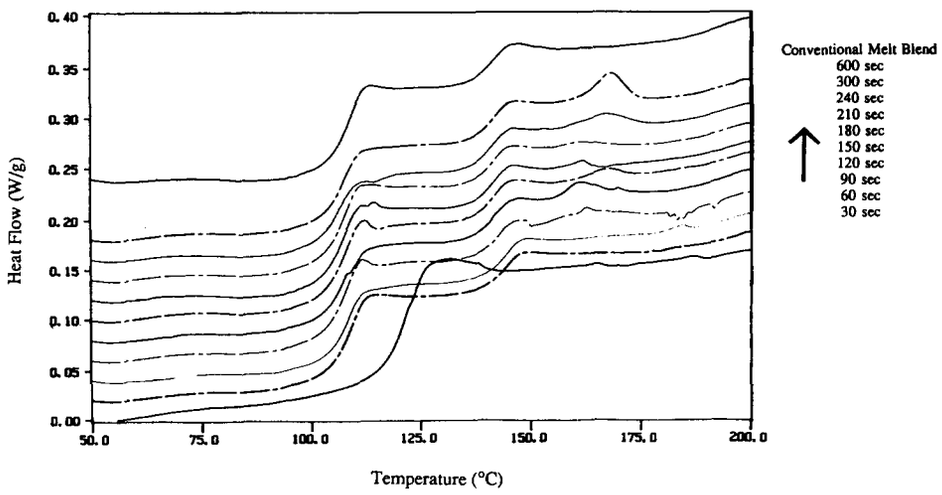

Figure 8 D.s.c. results for 50/50 BPACY/SAN25 *in situ* polymerized blends and conventional PC/SAN25 melt blend

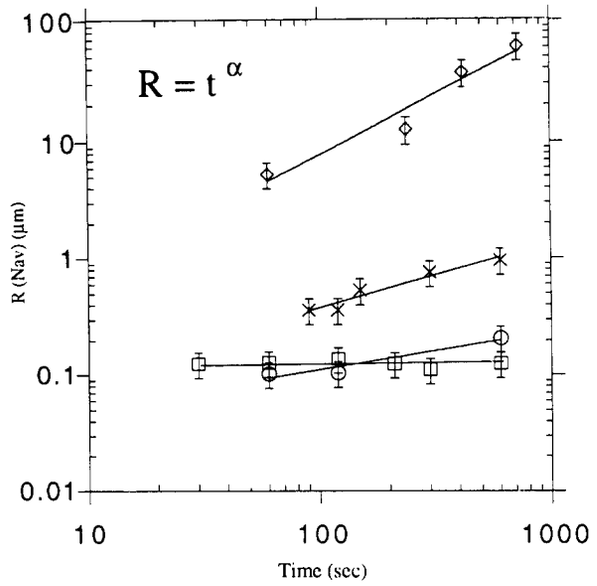

Figure 9 Number-average radius of dispersed domains *versus* time for *in situ* polymerized BPACY/SAN25 blends (0.07 mol% $(Bu)_4NH(Ph)_4$, 260°C). ◇, 70/30 ($\alpha = 1.00$); ×, 50/50 ($\alpha = 0.55$); □, 90/10 ($\alpha = 0.00$); ○, 10/90 ($\alpha = 0.33$)

late-stage coarsening of polymer systems has recently been questioned[69,70] and will be discussed below.

A diffusion-reaction type process for the late stage of coarsening initially proposed by Binder and Stauffer is an alternative mechanism to the evaporation–condensation of Ostwald ripening[66,71]. Smoluchowski kinetics are applied which treat each droplet as a free Brownian particle that will coalesce with another particle upon contact. This approach predicts scaling exponents which depend upon the balance of forces acting under particular experimental conditions as well as the volume fraction of dispersed phase. Scaling exponents, α, in the range $1/3 < \alpha < 1$ have been predicted. The balance between inertial and dissipative as well as between surface and thermal forces determines α. Fastest growth rates are expected for conditions where domains remain percolated throughout the coarsening process. The growth law exponent may change with time since the size of domains can affect the balance of forces acting upon them.

A variety of growth law scaling exponents have been observed in the demixing of polymer systems[66]. Critical mixtures consistently display $\alpha = 0$ for the early stages of demixing where the wavelength of composition fluctuations due to spinodal decomposition is expected to be constant. During the later stages, there is a gradual change in α with time until a relatively constant value of $0.8 < \alpha < 1$ is reached during late-stage coarsening. In contrast, the late-stage coarsening of off-critical mixtures has recently been shown to slow down with an eventual cessation of coarsening referred to as a 'pinning' of domain growth[69]. Scaling exponents for these off-critical mixtures have been shown to decrease from $\alpha \approx 0.8$ to $\alpha = 0$ during the late stage. This pinning has been attributed to a 'dynamical percolation to cluster transition'[69]. Domain coarsening during the late stage proceeds rapidly when domains percolate or form local clusters but this coarsening is slowed and finally arrested when dispersed domains become separated from each other in space. This phenomenon is unique to polymer systems due to an extreme barrier to coarsening via diffusive mechanisms. When a small molecule fluid undergoes a dynamical percolation to cluster transition it can still coarsen via diffusive mechanisms since barriers to diffusion through the matrix are low. For polymer systems, however, a large entropic barrier exists for transport across a sharp interface. Monte Carlo simulations by Kotnis and Muthukumar have recently demonstrated that the entropic barrier, unique to polymer systems, for transport across sharp interfaces can in fact result in a cessation of coarsening[70].

The phenomenon of 'pinning' unique to polymer systems is shown schematically in *Figure 10*. When the volume fraction of the dispersed phase is low, the dispersed domains exist as independent entities separated from each other in space. Under these conditions, coarsening can occur either by diffusion of material from a small particle through the matrix into a larger particle (i.e. diffusion perpendicular to a sharp interface) or by the diffusion of two domains into contact with each other. Extreme barriers exist to these processes in polymer systems, unlike similar processes in small molecule mixtures. As discussed above, the high molecular weight and connectivity of a polymer molecule result in a large entropic barrier to diffusion perpendicular to a sharp interface as well as a high viscosity which impedes diffusion of dispersed domains as free particles. As the volume fraction of the dispersed phase increases, the random placement of these domains forces some of them to come in contact with each other to form local clusters. These clusters can reduce their overall surface energy and coarsen without requiring the transport of polymer molecules across sharp interfaces or the large-scale translation of an entire domain. Thus, these local clusters can coarsen rapidly with time.

The 'pinning' of domain growth observed for the 90/10 BPACY blend is consistent with the above explanation.

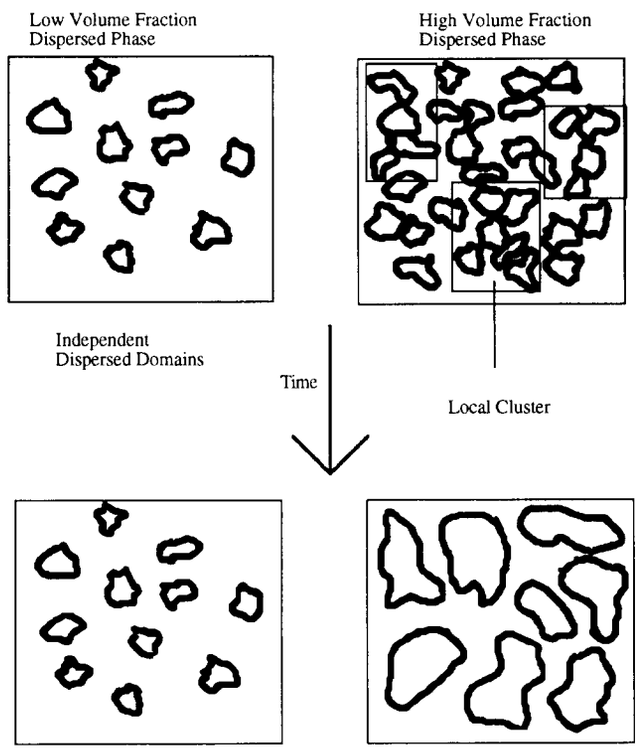

Figure 10 Schematic representation of the 'pinning' of domain coarsening

At this composition, the earliest stages of phase separation result in dispersed domains separated from each other in space; these domains do not form local clusters. The 60 s morphology (complete conversion) for the 90/10 system is shown in *Figure 11*. The later stage morphology (600 s), which is essentially unchanged, is shown in *Figure 12*. The dispersed SAN domains are independent of one another at this volume fraction. At higher volume fractions of dispersed phase (see *Figures 5a* to *g*) a random arrangement of domains results in the formation of local clusters in which a number of domains are in contact. The coarsening of these clusters can occur without transport across a sharp interface in contrast to dispersed independent domains at low volume fractions.

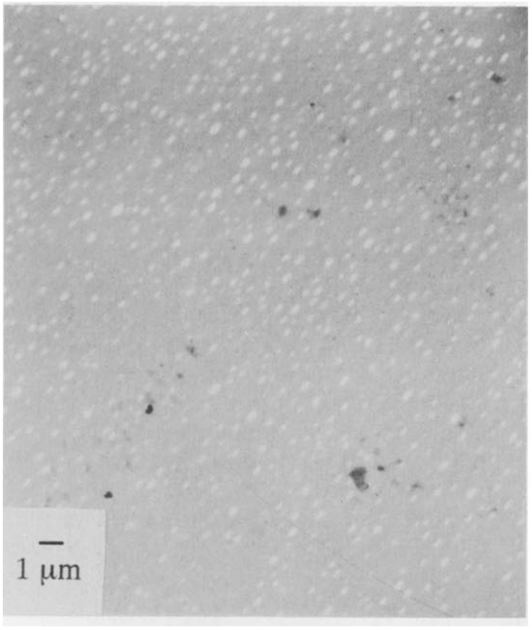

Figure 11 TEM micrograph of 90/10 BPACY/SAN25 blend containing 0.07 mol% $(Bu)_4NB(Ph)_4$ heat-treated at 260°C for 60 s

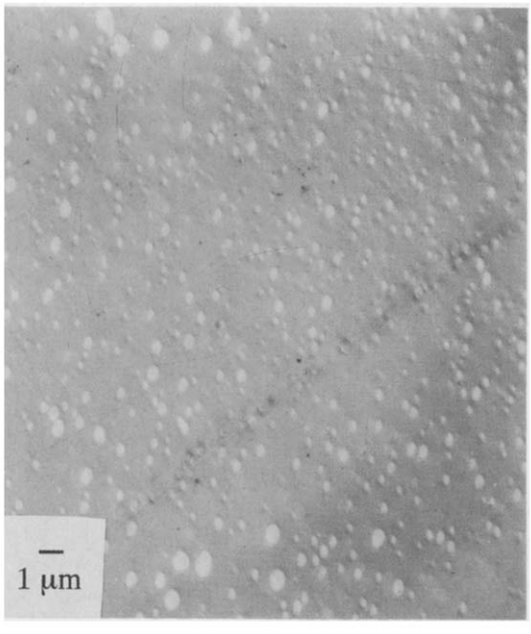

Figure 12 TEM micrograph of 90/10 BPACY/SAN25 blend containing 0.07 mol% $(Bu)_4NB(Ph)_4$ heat-treated at 260°C for 600 s

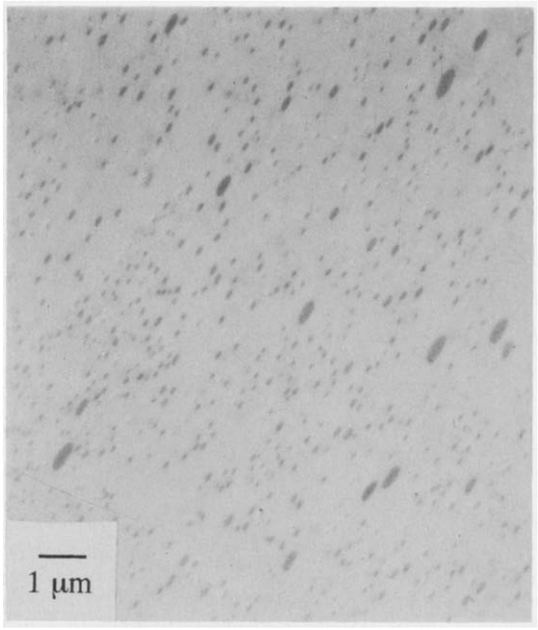

Figure 13 TEM micrograph of 10/90 BPACY/SAN25 blend containing 0.07 mol% $(Bu)_4NB(Ph)_4$ heat-treated at 260°C for 600 s

Although the 10/90 system also consists of independent dispersed particles, it did coarsen slightly over 600 s. In contrast to the 90/10 system, the 10/90 blend consists of PC-rich domains dispersed in a lower viscosity SAN-rich matrix (see *Figure 13*). The viscosity of PC at 260°C is 20 times that of SAN (16 000 poise *versus* 800 poise)[72]. The slight coarsening of the 10/90 system may be due to the lower viscosity of the matrix which presents less resistance to migration or transport of the dispersed domains as free particles resulting in a greater probability for the collision of two domains.

Dispersion-size effects on mechanical properties

The ability to prepare PC/SAN25 blends with varying morphologies via the *in situ* polymerization of BPACY/SAN blends enabled an investigation of the effect of dispersed-phase size on high-stress deformation behaviour. The effect of changes in the size of phase dispersion were expected to be greatest at blend compositions close to that at which a ductile–brittle 'transition' occurs under the chosen test conditions. Therefore, 70/30 BPACY/SAN25 blends containing 0.07 mol% $(Bu)_4NB(Ph)_4$ were heat-treated, as described previously, for various times followed by rapid quenching to below T_g. The BPACY were completely converted to PC ($M_w = 47\,000$, $M_w/M_n = 2.4$) in less than 60 s. The molecular weights of the resultant PC and the SAN25 were unaffected by longer heating times.

The morphology obtained after 60 s is shown in *Figure 14a*. SAN-rich domains (radii ≈ 4 μm) are dispersed in a PC-rich matrix. The morphology is uniform through the 0.080 cm thickness of the specimen, which reveals that thermal gradients are insignificant in these thin sheets. Note that *Figures 14a* to *d* display the morphology through the entire thickness of the specimen. Heat treatment for 240 s produced a coarsened morphology. There is also evidence for flow during this time-scale. The 240 s specimen was slightly thinner (0.07 cm) and the SAN-rich domains at the surfaces formed highly elongated 'threads' due to extensional flow at the

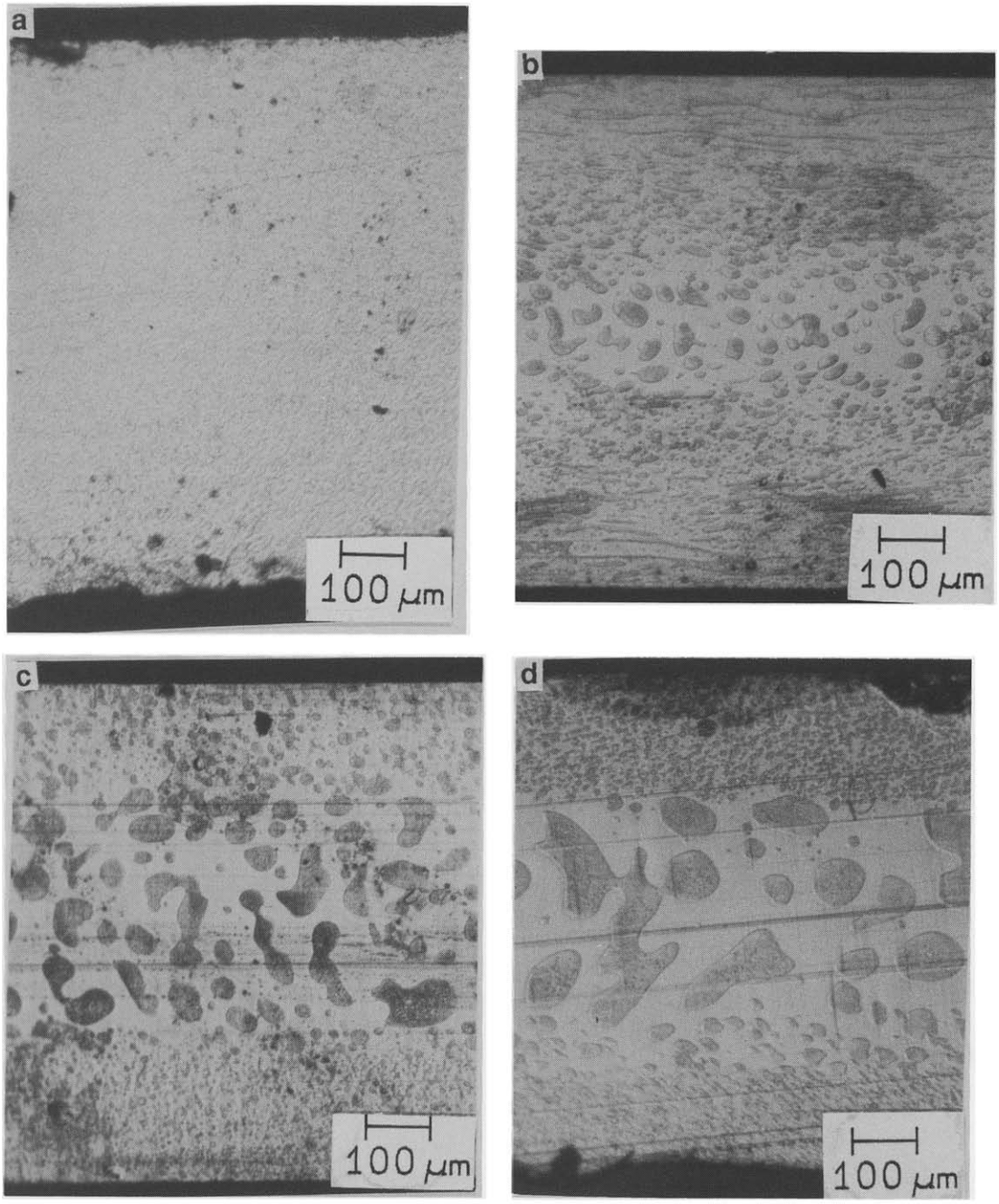

Figure 14 Photomicrograph of 70/30 BPACY/SAN25 blend containing 0.07 mol% $(Bu)_4NB(Ph)_4$ heat-treated at 260°C for various times. Entire specimen thickness shown from top to bottom of figure. (Surface microtomed, oxygen plasma etched and Pd/Au coated; bright-field reflected light illumination). (a) 60 s; (b) 240 s; (c) 420 s; (d) 720 s

specimen surfaces (see *Figure 14b*). This flow is due to the fact that the initial unconverted BPACY/SAN25 plaque is slightly thicker than the frame used during the final heat treatment. Thus, as 'flash' forms during the later stages of the heat treatment, the frame confines the resulting extensional flow to the surfaces of sheet which, in turn, results in the elongation of the SAN domains. In contrast, specimens prepared for phase-coarsening investigations were uniform through the thickness since a frame was not used in their preparation. Some elongation of the dispersed domains in these specimens was observed due to flow (see *Figures 5c–g*). This flow, however, was uniform through the specimen thickness. Moreover, this flow was not highly elongational and therefore did not produce thin threads. The 420 s morphology shown in *Figure 14c* reveals that the previously formed elongated threads at the surface have broken up into smaller spherical domains, presumably via capillary break-up driven by interfacial tension[73]. The domains in the interior have coarsened as expected and appear unaffected by the flow at the surface. Coarsening continues through 720 s (*Figure 14d*).

The tensile properties of the 70/30 blends were investigated for the range of morphologies described above. Homogeneous PC and SAN25 specimens which had been heat-treated at 260°C for the same times as the blends were also tested to determine whether the properties of the pure components change due to the

thermal treatment. Tensile tests were performed at two strain rates, $2.0 \times 10^{3}\,s^{-1}$ and $2.0 \times 10^{-4}\,s^{-1}$. Six specimens were tested at each strain rate for each morphology or thermal treatment. The results are summarized in *Table 1*.

Representative stress–displacement curves for PC at the two strain rates studied are shown in *Figure 15*. PC was ductile at both strain rates and showed the usual rate-dependent yield stress. The tensile behaviour of PC was independent of thermal treatment when held at 260°C for times between 60 and 720 s and then quenched. In contrast, SAN25 was brittle at both strain rates. Within experimental error, its breaking stress was independent of strain rate as well as thermal treatment. Representative stress–displacement curves are given in *Figure 16*.

All six specimens of 70/30 PC/SAN25 blend in which the PC had been polymerized *in situ* and held at 260°C for 60 s were ductile at the lower strain rate. The macroscopic yield stress was greater than that for PC. In all cases, deformation occurred without any observable crazing or stress whitening. In addition, a well developed neck formed as the specimens underwent cold drawing. Tests were terminated before fracture but after yielding and cold drawing. These observations imply that the SAN25 domains deformed via shear yielding, in contrast to the behaviour of SAN by itself which is brittle under uniaxial tension. At the greater strain rate only one specimen out of six underwent ductile yielding with the other five failing in a brittle manner. Representative stress–displacement curves for the 60 s morphology are given in *Figure 17*. As the morphology of the core section coarsens with longer thermal treatment times, fewer and fewer of the specimens were ductile until, after 720 s at 260°C, all specimens were brittle at both strain rates. The gradual loss of ductility at the lower strain rate with increasing size of the dispersed SAN domains is displayed in *Figure 18*. All specimens that yielded deformed without whitening and formed a well defined neck independent

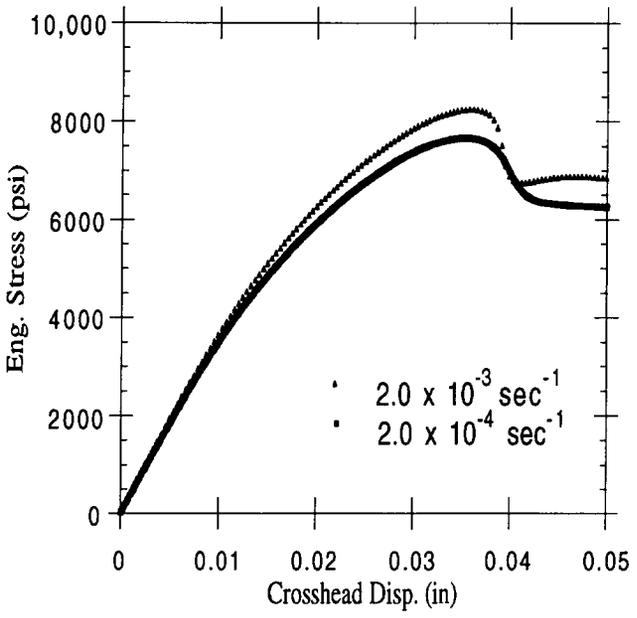

Figure 15 Representative stress–displacement curves for polycarbonate

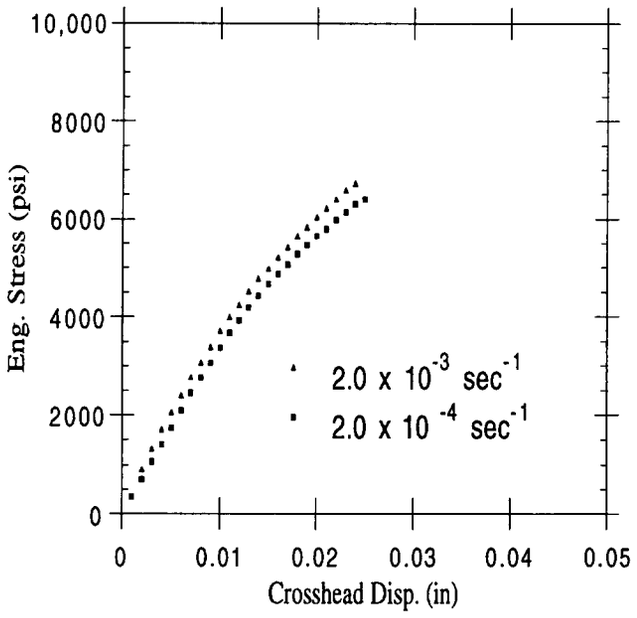

Figure 16 Representative stress–displacement curves for SAN25

Table 1 Tensile properties of *in situ* polymerized 70/30 BPACY/SAN25 blends and pure components

Material	Strain rate (s^{-1})	No. ductile	Yield stress (psi)	No. brittle	Breaking stress (psi)
PC[a]	2.0×10^{-4}	6	7800 ± 200	0	–
	2.0×10^{-3}	6	8400 ± 200	0	–
SAN25[a]	2.0×10^{-4}	0	–	6	6200 ± 300
	2.0×10^{-3}	0	–	6	6400 ± 300
70/30 60 s	2.0×10^{-4}	6	8600 ± 300	0	–
	2.0×10^{-3}	1	9000	5	9000 ± 300
70/30 240 s	2.0×10^{-4}	4	8300 ± 200	2	7500 ± 200
	2.0×10^{-3}	0	–	6	8600 ± 200
70/30 420 s	2.0×10^{-4}	3	8500 ± 200	3	7800 ± 500
	2.0×10^{-3}	0	–	6	8800 ± 200
70/30 720 s	2.0×10^{-4}	0	–	6	7800 ± 400
	2.0×10^{-3}	0	–	6	7800 ± 300

[a] The tensile properties of PC and SAN25 were independent of heat treatment time at 260°C. The PC used was a commercial injection moulding grade resin ($M_w = 44\,000$, $M_w/M_n = 2.5$)

of heat-treatment time. Specimens that failed in a brittle manner did so without any visible damage away from the fracture surface.

In order to confirm that dispersed SAN25 domains underwent shear yielding when specimens yielded macroscopically, sections for TEM were microtomed parallel to the tensile axis from within both an undeformed region as well as the necked region. *Figure 19a* displays the undeformed morphology for a 70/30 blend held at 260°C for 240 s while the morphology within the neck is shown in *Figure 19b*. The SAN domains have clearly been oriented and elongated along the tensile direction. In addition there is no evidence for crazing within the SAN domains nor is there any debonding at the PC/SAN interfaces. An optical micrograph of a larger area which displays the morphology on both sides of the neck is given in *Figure 20*. This also demonstrates the orientation and elongation of the SAN due to shear flow.

The deformation below a brittle fracture surface was also investigated by microtoming sections perpendicular to the fracture surface of broken specimens embedded in epoxy and stained with OsO_4 prior to sectioning. *Figure 21a* displays a low-magnification transmission electron micrograph of the region directly below the fracture surface of a specimen held at 260°C for 720 s. The finer morphology is observed at the skin with large

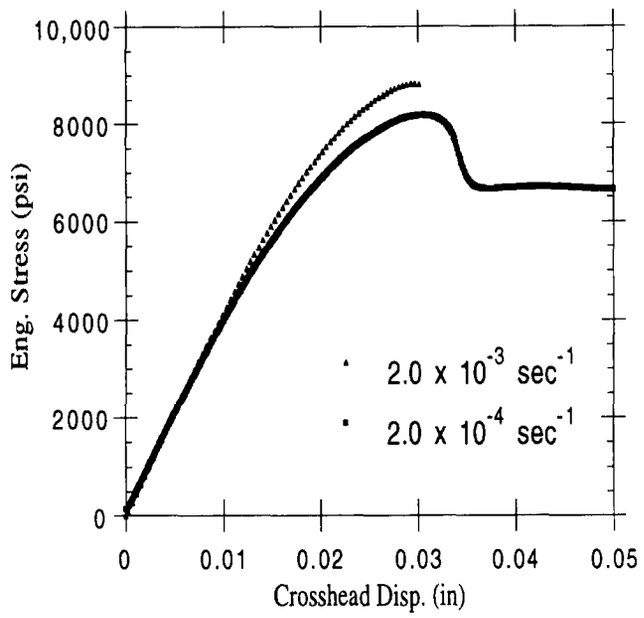

Figure 17 Representative stress–displacement curves for a 70/30 BPACY/SAN25 blend containing 0.07 mol% $(Bu)_4NB(Ph)_4$ heat-treated at 260°C for 60 s

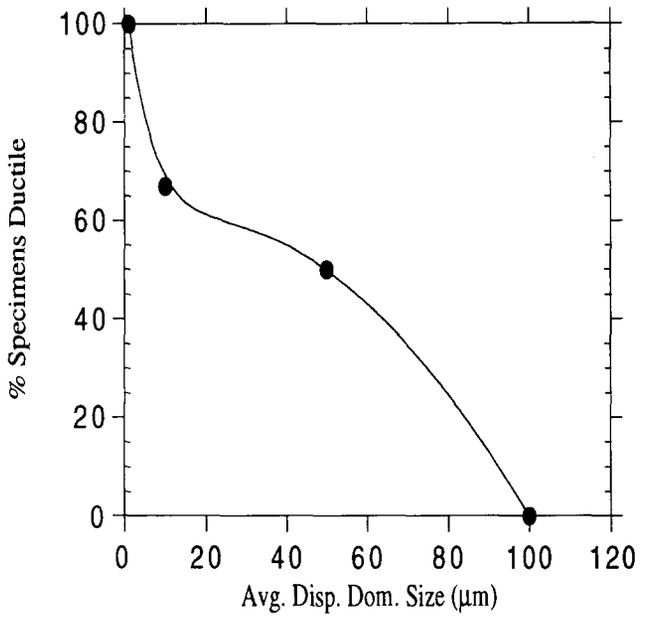

Figure 18 Effect of dispersed domain size on the deformation of 70/30 PC/SAN blends

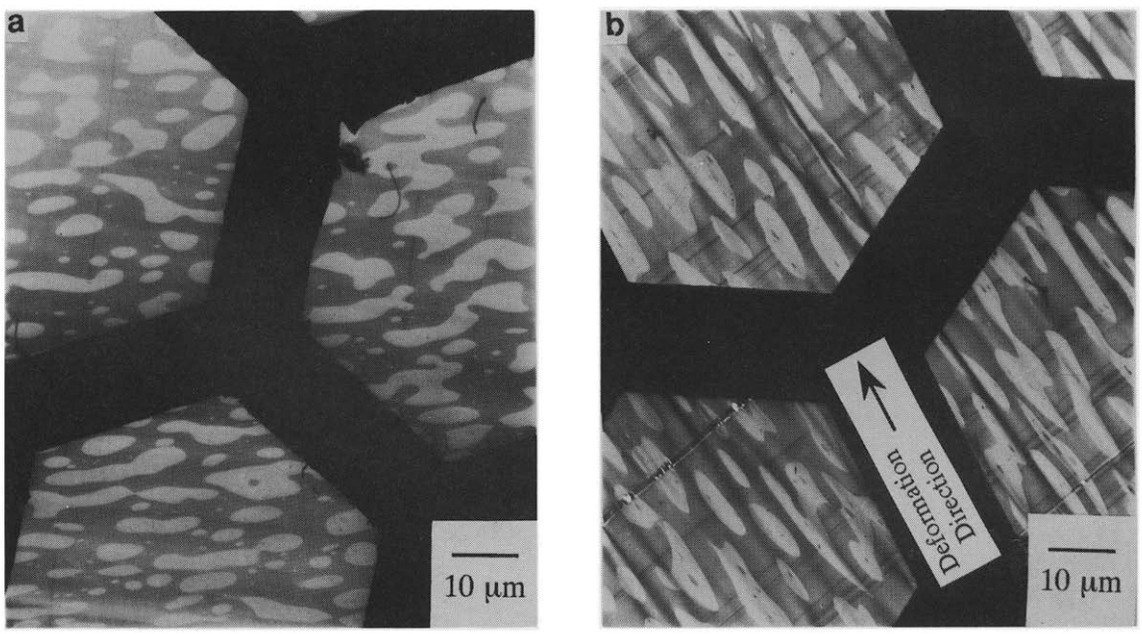

Figure 19 TEM micrographs 70/30 BPACY/SAN25 blend containing 0.07 mol% $(Bu)_4NB(Ph)_4$ heat-treated at 260°C for 240 s. (a) Undeformed region; (b) necked region. (Note that copper grid bars are visible)

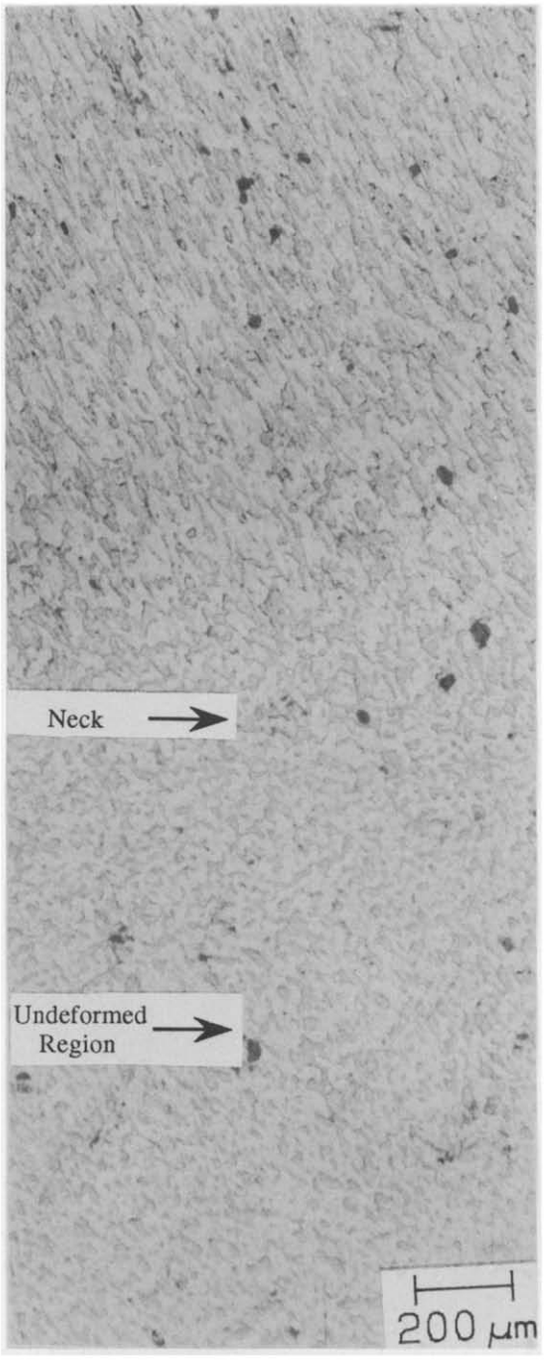

Figure 20 Photomicrograph of 70/30 BPACY/SAN25 blend containing 0.07 mol% $(Bu)_4NB(Ph)_4$ heat-treated at 260°C for 240 s. Figure includes deformed and non-deformed regions on either side of neck. (Surface microtomed, oxygen plasma etched and Pd/Au coated; bright-field reflected light illumination)

SAN domains in the core. A large SAN domain that has apparently been split in two is seen at the fracture surface. A detailed view of this large SAN domain (*Figure 21b*) reveals a large number of internal crazes parallel to the fracture surface that terminate at the SAN/PC interface. Crazing was evident only in the region immediately below the fracture surface with no damage evident more than about 50 μm below the fracture surface. In addition, smaller SAN domains showed a lower tendency to craze.

Arrested cleavage crack tips were prepared in both the 60 s and 720 s morphologies in order to understand better the transition from ductile to brittle behaviour as the SAN dispersion coarsens. Sections for optical microscopy were prepared by petrographically thinning a cracked specimen from both surfaces to yield a thin section centred at the midplane. These sections were then imaged by a variety of optical methods. Bright-field reflection images of the crack tips in the 60 s and 720 s morphologies are shown in *Figures 22a* and *b*. The size of the dispersed SAN domains is seen to have a significant effect on the nature of the crack tip. The crack tip in the finer morphology (60 s, *Figure 22a*) is bifurcated with little damage evident in the region surrounding the crack tip. The crack propagates directly through SAN domains at this plane but does not pass through the PC matrix.

The bright-field reflection image of the crack tip in the central region of the 720 s morphology (*Figure 22b*) reveals that cavitation does occur in the PC as the crack propagates. The region ahead of this crack tip contains many small cracks that have split SAN domains as well as propagated into the PC matrix. This behaviour stands in sharp contrast to the behaviour of the crack in the specimen with a finer dispersion of SAN. Although it is not possible to determine where these cracks initiated, we suspect that the cracks initiated in the SAN-rich domains since the crazing resistance of SAN is lower than that of PC[74]. It appears that the large SAN domains are more prone to crazing and cracking and that when these cracks form they propagate into the PC matrix. New cracks do not seem to initiate in the smaller SAN domains ahead of the macroscopic crack tip and do not appear to cause cavitation in the PC matrix ahead of the crack tip. The dark-field reflection micrographs (*Figures 23a* and *b*) provide another view of the thin cracks ahead of the crack tip in the 720 s specimen in contrast to the 60 s morphology.

Images of the two crack tips between crossed polars provide further insight into the influence of particle size on high-stress deformation mechanisms. The crack tip in the 720 s specimen is shown in *Figure 24b*. The central region of the crack itself is the only region which is birefringent. The region ahead of the crack is clearly not birefringent, which implies that no shear flow has occurred. Recall that the images in bright- and dark-field reflection (*Figures 22b* and *23b*) revealed that cavitational deformation mechanisms were active in response to the stress field in this region. In contrast, the crack in the specimen containing the finer dispersion of SAN is surrounded by highly birefringent material (see *Figure 24a*). This confirms that shear flow has occurred in the ligaments of PC between the cracked SAN domains as noted above. In addition, the region ahead of the bifurcated crack tip is highly birefringent. This confirms that instead of cavitation (i.e. cracking) in response to the stress field, the finer morphology results in shear deformation.

The effect of dispersed domain size in blends of a brittle polymer dispersed in a more ductile matrix described in this work is similar to that observed by others. Two possible mechanisms have been proposed for the transition from brittle to ductile behaviour as a brittle phase becomes more finely dispersed in a ductile matrix as found in this work. These mechanisms, which are not mutually exclusive, are listed below.

1. Berger and Kramer have proposed that crazing is suppressed in small domains (~ 1 μm) because formation of craze fibrils at the craze tip is suppressed[75].

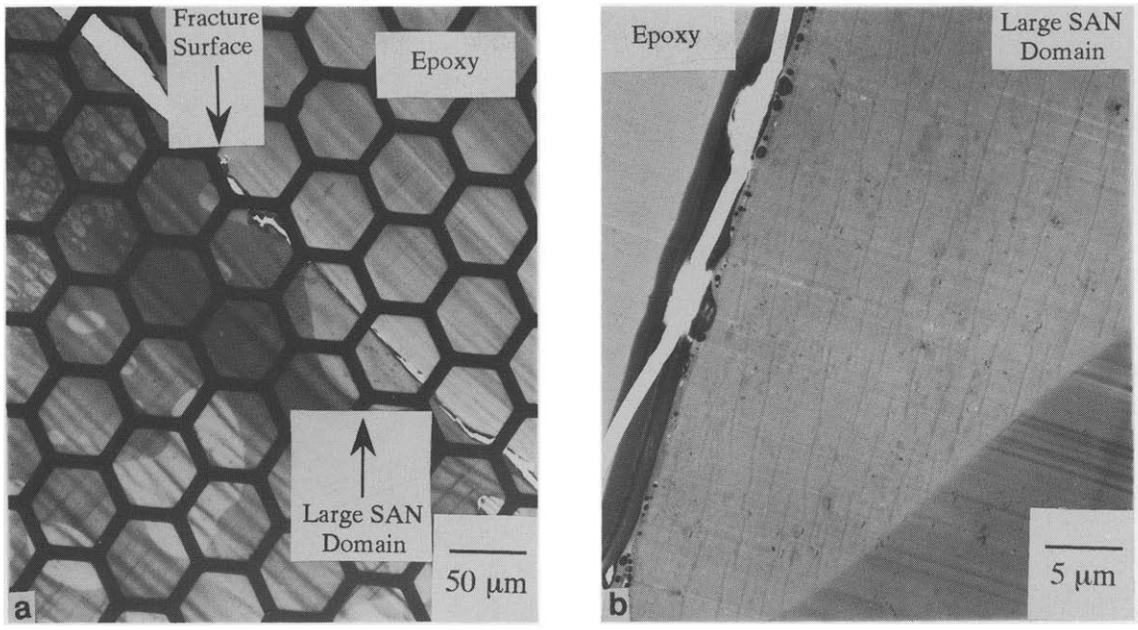

Figure 21 TEM micrograph of brittle fracture surface of a 70/30 BPACY/SAN25 blend containing 0.07 mol% $(Bu)_4NH(Ph)_4$ heat-treated at 260°C for 720 s. (Epoxy embedded, stained with OsO_4 to highlight crazes). (a) Low magnification; (b) close-up of large SAN domain at fracture surface

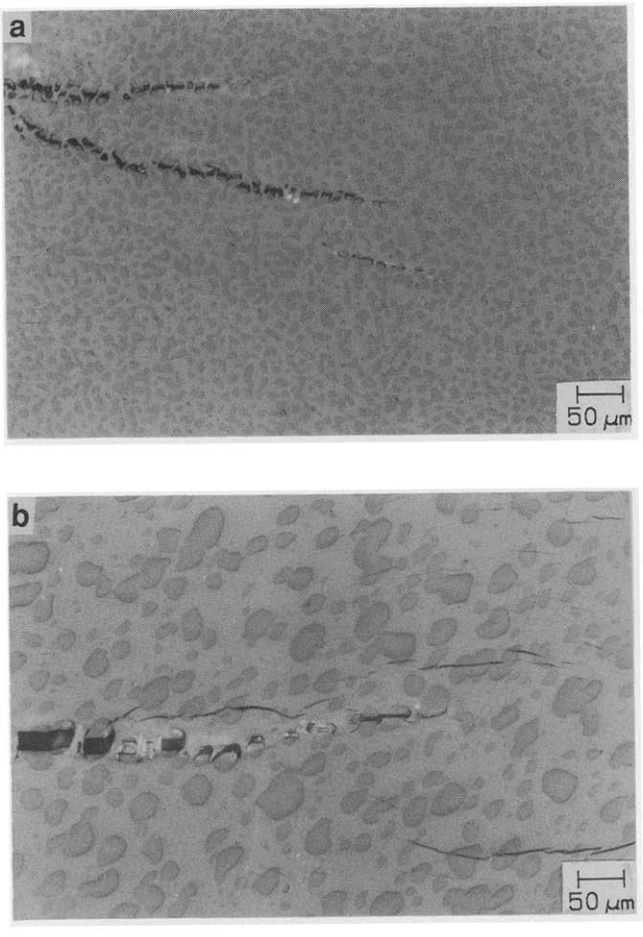

Figure 22 Bright-field reflection photomicrographs of arrested crack tips in *in situ* polymerized 70/30 BPACY/SAN25 blends. (a) 60 s morphology; (b) 720 s morphology. (Thin sections of specimen mid-plane)

These authors propose that in order for a craze to form, the volume of an inclusion must be at least an order of magnitude greater than fibril spacings, which are typically 0.02 to 0.1 μm. Thus the smaller the inclusion the greater the restriction to craze formation which is the antecedent of brittle failure.

2. When a dispersed brittle domain does crack, the stress concentration at the interface between it and the matrix will depend strongly on the length of the crack[76]. The smaller the dispersed domain the lower will be the stress concentration at the interface between it and the matrix when that domain has cracked[76]. Thus when a crack forms in a small dispersed phase the likelihood of it propagating into the matrix is reduced relative to a crack in a larger domain. The work of Berger and Kramer[75] and Ma *et al.*[51], in addition to that presented here has shown that small crazes/cracks formed in the SAN can be blunted by shear flow in the PC matrix while larger cracks propagate into the matrix. In effect the smaller domains isolate the effect of heterogeneous craze initiation sites.

Conceivably, the enhanced ductility of a finely dispersed brittle phase is best understood as the synergistic result of the effects described above.

SUMMARY

The *in situ* polymerization of BPACY/SAN blends has been demonstrated to yield PC/SAN blends with morphologies unattainable via conventional melt blending. Extremely fine phase dispersion can be obtained by this method of blend preparation. The domain-coarsening kinetics have been shown to be quite sensitive to the

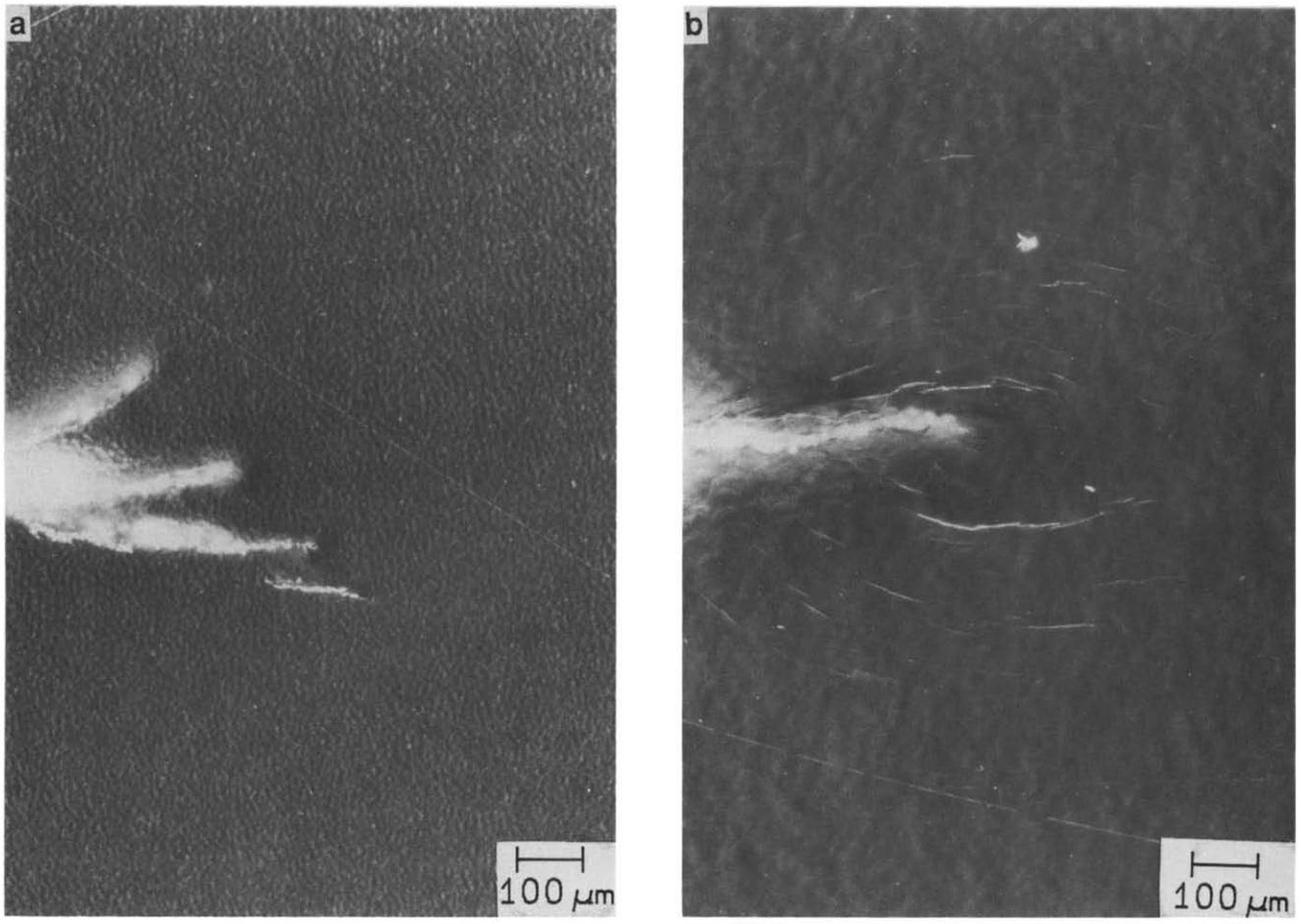

Figure 23 Dark-field reflection photomicrographs of arrested crack tips in *in situ* polymerized 70/30 BPACY/SAN25 blends. (a) 60 s morphology; (b) 720 s morphology. (Thin sections of specimen mid-plane)

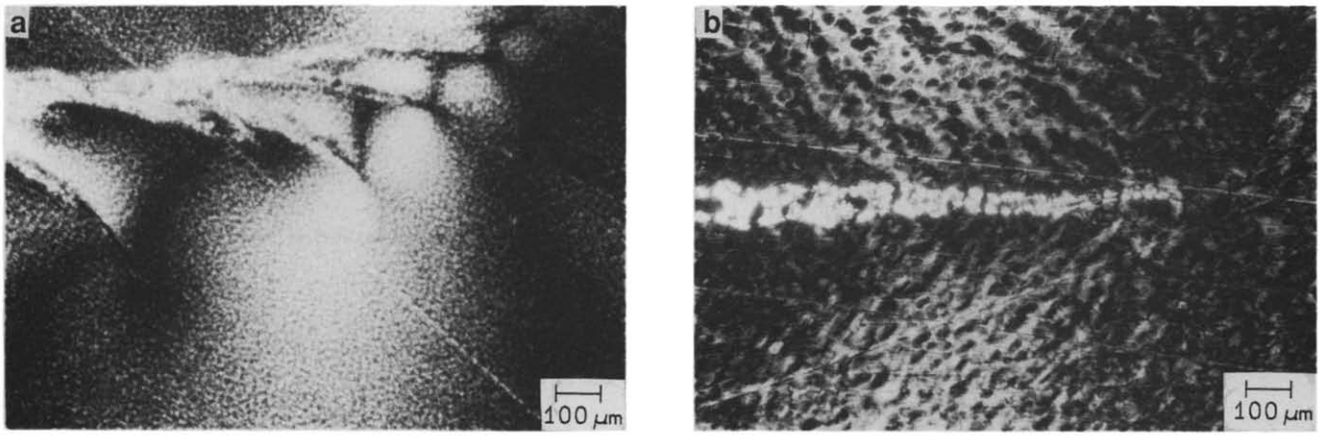

Figure 24 Photomicrographs of arrested crack tips in *in situ* polymerized 70/30 BPACY/SAN25 blends viewed between crossed polars. (a) 60 s morphology; (b) 720 s morphology. (Thin sections of specimen mid-plane)

volume fraction of the dispersed phase. The 'pinning' of domain coarsening, unique to polymer systems, can be attributed to the extreme barriers to diffusive coarsening mechanisms in these systems. Thus phase coarsening is arrested when percolation ceases or domains no longer form local clusters.

The dispersed-phase size has been shown to have a dramatic effect on high-stress deformation in systems where a brittle phase is dispersed in a more compliant ductile matrix. The increased ductility of blends with finer phase dispersions has been rationalized based on a lower tendency for smaller brittle phases to craze/crack in addition to the influence of complex local stress fields in heterogeneous materials.

ACKNOWLEDGEMENT

This work was conducted by W. L. N. at General Electric Corporate Research and Development in partial fulfilment of the requirements for a PhD at the University of Massachusetts. The authors thank General Electric for its financial support of this work.

REFERENCES

1 Utracki, L. A. 'Polymer Alloys and Blends: Thermodynamics and Rheology', Hanser, New York, 1989
2 Solc, K. (Ed.) 'Polymer Compatibility and Incompatibility: Principles and Practices', MMI, New York, 1982
3 Paul, D. R. and Newman, S. (Eds) 'Polymer Blends', Academic Press, New York, 1978, Vols 1 and 2
4 Olabisi, O., Robeson, L. M. and Shaw, M. T. 'Polymer–Polymer Miscibility', Academic Press, New York, 1979
5 Lindsay, G. A., Singleton, C. J. and Smith, R. W. *Adv. Chem. Ser.* 1979, **176**, 367
6 Bucknall, C. B. 'Toughened Plastics', Applied Science, London, 1977
7 Platt, A. E. in 'Comprehensive Polymer Science', (Eds G. Allen and J. C. Bevington), Pergamon, New York, 1989
8 Molau, G. E. *J. Polym. Sci.* 1965, **A3**, 1267
9 Molau, G. E. *J. Polym. Sci.* 1965, **A3**, 4235
10 Molau, G. E., Wittbrodt, W. M. and Meyer, V. E. *J. Appl. Polym. Sci.* 1969, **13**, 2735
11 Molau, G. E. and Keskkula, A. *Appl. Polym. Symp.* 1968, **7**, 35
12 Parent, R. R. and Thompson, E. V. *Adv. Chem. Ser.* 1979, **176**, 381
13 Parent, R. R. and Thompson, E. V. *J. Polym. Sci., Polym. Phys. Edn* 1978, **16**, 1829
14 Scott, R. L. *J. Chem. Phys.* 1949, **17**, 279
15 Tompa, H. 'Polymer Solutions', Butterworths, London, 1956
16 Flory, P. J. 'Principles of Polymer Chemistry', Cornell University Press, Ithaca, NY, 1959
17 Avny, Y., Rebenfeld, L. and Weigmann, H. D. *J. Appl. Polym. Sci.* 1978, **22**, 1978
18 Moshonov, A. and Avny, Y. *J. Appl. Polym. Sci.* 1980, **25**, 89
19 Lawton, E. L., Murayama, T., Holland, V. F. and Felty, D. C. *J. Appl. Polym. Sci.* 1980, **25**, 187
20 Doube, C. P. and Walsh, D. J. *Polymer* 1979, **20**, 1115
21 Walsh, D. J. and McKeown, J. G. *Polymer* 1980, **21**, 1330
22 Walsh, D. J. and Cheng, G. L. *Polymer* 1982, **23**, 1965
23 Walsh, D. J. and Cheng, G. L. *Polymer* 1984, **25**, 485
24 Walsh, D. J. and Sham, C. K. *Polymer* 1984, **25**, 1023
25 Chen, F.-L., Pearce, E. M. and Kwei, T. K. *Polymer* 1988, **29**, 2285
26 Wang, L. F., Pearce, E. M. and Kwei, T. K. *Polymer* 1991, **32**, 1991
27 Yau, H. and Stupp, S. I. *J. Polym. Sci., Polym. Chem. Edn* 1985, **23**, 813
28 Galvin, M. E. and Heffner, S. A. *Macromolecules* 1986, **19**, 2461
29 Galvin, M. E. and Heffner, S. A. *Macromolecules* 1988, **21**, 1895
30 Galvin, M. E. and Wnek, G. E. *J. Polym. Sci., Polym. Chem. Edn* 1983, **21**, 2727
31 Kiss, G., Kovacs, A. J. and Wittmann, J. C. *J. Appl. Polym. Sci.* 1981, **26**, 2665
32 Sperling, L. H. 'Interpenetrating Polymer Networks and Related Materials', Plenum, New York, 1981
33 Sperling, L. H. in 'Comprehensive Polymer Science' (Eds G. Allen and J. C. Bevington), Pergamon, New York, 1989
34 Kurauchi, T. and Ohta, T. *J. Mater. Sci.* 1984, **19**, 1699
35 Sue, H. J., Pearson, R. A. and Yee, A. F. *Polym. Eng. Sci.* 1991, **31**, 793
36 Goodier, J. N. *J. Appl. Mech.* 1933, **55**, 39
37 Wang, T. T., Matsuo, M. and Kwei, T. K. *J. Appl. Phys.* 1971, **42**, 4188
38 Sternstein, S. S. and Myers, F. A. *J. Macromol. Sci. Phys. B* 1973, **8**, 539
39 Biglione, G., Baer, E. and Radcliffe, S. V. 'Proc. 2nd Int. Conf. on Fracture', Chapman and Hall, London, 1969
40 Bheteja, S. K. and Pae, K. D. *Polym. Lett.* 1972, **10**, 531
41 Matsushige, K., Baer, E. and Radcliffe, S. V. *J. Macromol. Sci. Phys. B* 1975, **11**, 565
42 Matsushige, K., Radcliffe, S. V. and Baer, E. *J. Appl. Polym. Sci.* 1976, **20**, 1853
43 Ishikawa, M. and Narisawa, I. *J. Mater. Sci.* 1983, **18**, 1947
44 Koo, K. K., Inoue, T. and Miyasaka, K. *Polym. Eng. Sci.* 1985, **25**, 741
45 Angola, J. C., Fujita, Y., Sakai, T. and Inoue, T. *J. Polym. Sci., Polym. Phys. Edn* 1988, **26**, 807
46 Quintens, D., Groeninckx, G., Guest, M. and Aerts, L. *Polym. Eng. Sci.* 1990, **30**, 1474
47 Quintens, D., Groeninckx, G., Guest, M. and Aerts, L. *Polym. Eng. Sci.* 1990, **30**, 1484
48 Quintens, D., Groeninckx, G., Guest, M. and Aerts, L. *Polym. Eng. Sci.* 1991, **31**, 1215
49 Kim, W. Y. and Lee, D. S. *Polym. Bull.* 1991, **26**, 701
50 Gregory, B. L., Siegman, A., Im, J., Hiltner, A. and Baer, E. *J. Mater. Sci.* 1987, **22**, 532
51 Ma, M., Vijayan, K., Hiltner, A., Baer, E. and Im, J. *J. Mater. Sci.* 1990, **19**, 2039
52 Im, J., Baer, E. and Hiltner, A. in 'High Performance Polymers', (Eds E. Bear and A. Moet), Hanser, New York, 1991
53 Brunelle, D. J., Bowden, E. P. and Shanon, T. G. *J. Am. Chem. Soc.* 1990, **117**, 2399
54 Brunelle, D. J. and Shannon, T. G. *Macromolecules* 1991, **24**, 3035
55 Brunelle, D. J. in 'Ring Opening Polymerization' (Ed. D. J. Brunelle), Hanser Verlag, Munich, Ch. 11
56 Evans, T. L., Berman, C. B., Carpenter, J. C., Choi, D. Y. and Williams, D. A. *Polym. Prepr.* 1989, **30** (2), 573
57 Stewart, K. R. *Polym. Prepr.* 1989, **30** (2), 575
58 Holik, A. S., Kambour, R. P., Fink, D. G. and Hobbs, S. Y. *Microstruct. Sci.* 1979, **7**, 357
59 Keitz, J. D., Barlow, J. W. and Paul, D. R. *J. Appl. Polym. Sci.* 1984, **29**, 3131
60 Cahn, J. W. in 'Dynamics of Ordering Processes in Condensed Matter' (Eds S. Komura and H. Furukawa), Plenum Press, New York, 1987
61 Siggia, E. D. *Phys. Rev. A* 1979, **20**, 595
62 Gunton, J. D., San Miguel, M. and Sahni, P. S. in 'Phase Transitions and Critical Phenomena' (Eds C. Domb and J. L. Lebowitz), Vol. 8, Academic Press, New York, 1983
63 Hashimoto, T. in 'Current Topics in Polymer Science' (Eds R. M. Ottenbrite, L. A. Utracki and S. Inoue), Vol. 2, Hanser, New York, 1987
64 Hashimoto, T. *Phase Transitions* 1988, **12**, 47
65 Han, C. in 'Molecular Conformation and Dynamics of Macromolecules in Condensed Systems' (Ed. M. Nagasawa), Elsevier, Amsterdam, 1988
66 Furukawa, H. *Adv. Phys.* 1985, **34**, 703
67 Lifshitz, I. M. and Slyozov, V. V. *J. Phys. Chem. Solids* 1961, **19**, 35
68 Wagner, C. *Z. Electrochemistry* 1961, **65**, 581
69 Hashimoto, T., Takenaka, M. and Izumitani, T. *J. Chem. Phys.* 1992, **97**, 679
70 Kotnis, M. and Muthukumar, M. *Macromolecules* 1992, **25**, 1716
71 Binder, K. and Stauffer, D. *Phys. Rev. Lett.* 1974, **33**, 1006
72 Richards, W. D. personal communication
73 Tomotika, S. *Proc. R. Soc. Ser. A* 1935, **150**, 322
74 Kambour, R. P. *Polym. Commun.* 1985, **24**, 292
75 Berger, L. L. and Kramer, E. J. *J. Mater. Sci.* 1987, **22**, 2739
76 Hiroshi, T., Paris, P. C. and Irwin, G. R. 'The Stress Analysis of Cracks Handbook', Paris Productions, St Louis, MO, 1985